Accretion of the relativistic Vlasov gas onto a Kerr black hole

Ping Li,[1,*] Yong-qiang Liu,[2,†] and Xiang-hua Zhai[2,‡]

[1]*College of Mathematics and Physics, Hunan University of Arts and Sciences, 3150 Dongting Dadao, Changde City, Hunan Province 415000, China*

[2]*Division of Mathematica and Theoretical Physics, Shanghai Normal University, 100 Guilin Road, Shanghai 200234, China*

(Received 23 August 2023; accepted 16 November 2023; published 7 December 2023)

We study the accretion of relativistic Vlasov gas onto a Kerr black hole, regarding the particles as distributed throughout all of the space, rather than just in the equatorial plane. We solve the relativistic Liouville equation in the full $3+1$-dimensional framework of Kerr geometry. For the stationary and axially symmetric flow, we prove that the distribution function is independent of the conjugate coordinates. For an explicit distribution that can be approximated as a Maxwell-Jüttner distribution, we further calculate the particle current density, stress-energy-momentum tensor, and unit accretion rates of mass, energy, and angular momentum. The analytic results at large distance are shown to be consistent with the limits of the numerical ones computed at finite distance. In particular, we show that the unit mass accretion rate agrees with the Schwarzschild result in the case of the low-temperature limit. Furthermore, we find from the numerical results that the three unit accretion rates vary with the angle in the Kerr metric and the accretion of Vlasov gas would slow down the Kerr black hole. The closer to the equator, the faster it slows down the black hole.

DOI: 10.1103/PhysRevD.108.124022

I. INTRODUCTION

An ensemble composed of a large number of massive particles that only interact with each other through gravitation is called a Vlasov gas. The distribution function of such an ensemble satisfies the collisionless Liouville equation, also called the Vlasov equation in mathematics. Vlasov models have a long history in astrophysics. The Newtonian systems are often used to model galaxies [1] and globular clusters [2]. The relativistic Vlasov gas is often chosen to be the matter when investigating open problems in general relativity, such as the cosmic censorship hypotheses [3]. In particular, in the strong-gravity areas, such as the galaxies' center, the interest in studying relativistic Vlasov gas is increasing [4,5]. For recent reviews, we refer to [6].

It is claimed that the gas surrounding M87 or Sgr A*, both of which are astronomical black holes observed by the Event Horizon Telescope Collaboration, is also nearly collisionless and magnetized [7–11]. In Refs. [12,13], Rioseco and Sarbach performed a detailed study of the accretion of Vlasov gas onto a Schwarzschild black hole. They solved the relativistic Liouville equation in Schwarzschild geometry and obtained the condition satisfied by the distribution function with an appropriate symmetry. In a particular model with a spherical steady-state flow, they derived the current density and the stress-energy-momentum tensor. Such a relativistic Vlasov model is also used to provide a partial explanation for the low accretion rate problem, also called the Bondi-Hoyle-Lyttleton (BHL) accretion problem [14–17].

Since then, numerous works have extended such a model to more general situations. Cieślik and Mach generalized Rioseco and Sarbach's results to Reissner-Nordström black holes [18]. In Refs. [19–21], the authors calculated the accretion of relativistic Vlasov gas onto a moving Schwarzschild black hole and tried to resolve the BHL accretion problem. The accretion of Vlasov gas onto a Schwarzschild black hole at a sphere of finite radius was also studied by Gamboa *et al.* [22]. Except for Schwarzschild black holes, Rioseco and Sarbach's results have also been extended to black holes in modified gravities. Liao and Liu investigated the accretion of a collisionless Vlasov gas onto a Bardeen regular black hole [23]. Cai and Yang studied the accretion of Vlasov gas onto black holes in bumblebee gravity [24]. There are also many studies of accretion onto Kerr black holes. Reference [25] showed that a collisionless, relativistic kinetic gas configuration propagating in the equatorial plane of a Kerr black hole would eventually settle down to a stationary, axisymmetric configuration surrounding the black hole. In the slowly rotating case, Ref. [26] proved the

*Lip57120@huas.edu.cn
†1000511286@smail.shnu.edu.cn
‡zhaixh@shnu.edu.cn

 © 2023 American Physical Society

decay of a bounded energy and integrated energy for massless Vlasov gas in Kerr spacetime. More recently, Cieślik *et al.* performed a detailed study of the accretion of Vlasov gas onto a Kerr black hole, occurring in the equatorial plane [27]. In Ref. [28], Mach *et al.* studied equatorial accretion on a moving Kerr black hole.

However, the studies of Vlasov gas accreting onto Kerr black holes so far have utilized the result of the distribution function of Vlasov gas obtained in Ref. [12], which is one of the solutions of the collisionless Liouville equation in Schwarzschild geometry. When considering the accretion onto a Kerr black hole, it is reasonable that the distribution function is the solution of the Liouville equation in Kerr geometry. In this paper, we solve the relativistic Liouville equation in the full $3+1$-dimensional frame of Kerr geometry and show that the general solution of the Liouville equation in Kerr geometry is different from the axisymmetric case in Schwarzschild geometry. On the other hand, since the total angular momentum L^2 is conserved in Schwarzschild geometry, it is reasonable to consider the time-like geodesic bounded to a single plane. However, things become different when working in Kerr geometry where the conserved quantity is the Carter constant D rather the total angular momentum L^2. It is not enough to work in the $2+1$ framework when talking about the accretion of Vlasov gas in Kerr geometry. In this paper, we discuss this issue in a full $3+1$ framework. Then, the particle current density J_μ and the stress-energy-momentum tensor $T_{\mu\nu}$ depend on both the radius r and angle θ. Therefore, when talking about the accretion of Vlasov gas in Kerr geometry, it is more complete to work in a full $3+1$ framework than to consider only the equatorial plane.

This paper is organized as follows. In Sec. II we review the Hamiltonian description of time-like geodesics in Kerr geometry. In Sec. III we solve the relativistic Liouville equation in a Kerr background and prove that the distribution function only depends on the canonical momentum P_μ. Furthermore, we simplify the volume element in both the nonequatorial and equatorial plane. In the special case that the 2-surface is a spherical surface, we obtain the expressions for the three accretion rates per unit surface. In Sec. IV we consider an explicit collisionless flow in a stationary state and with axial symmetry that can be approximated as a Maxwell-Jüttner distribution at infinity. The expressions for the particle current density J_μ and the stress-energy-momentum tensor $T_{\mu\nu}$ are computed. The limits of integration are discussed. In Sec. V we analytically examine the asymptotic behavior at large distances where the corresponding quantities are all independent of the angle θ. Using a Taylor expansion of $\frac{1}{r}$, the leading terms and second terms of the unit accretion rates are computed. In Sec. VI we numerically compute the corresponding quantities in finite ranges. The last section is a detailed conclusion. In this paper, we use the units $G = c = 1$.

II. REVIEW OF GEODESIC MOTION IN KERR SPACETIME

A. Hamilton formulas of geodesic motion in Kerr spacetime

The geodesic motion in Kerr spacetime has been widely discussed in many papers and books. In this section, we give a brief review. This is done in Boyer-Lindquist coordinates (t, r, θ, φ), where the Kerr metric can be written as

$$ds^2 = \left(1 - \frac{2Mr}{\rho^2}\right)dt^2 + \frac{4Mar\sin^2\theta}{\rho^2}dtd\varphi - \frac{\rho^2}{\Delta}dr^2 - \rho^2 d\theta^2 - \frac{\sin^2\theta}{\rho^2}\Sigma^2 d\varphi^2, \tag{1}$$

where

$$\rho^2 = r^2 + a^2\cos^2\theta, \tag{2}$$

$$\Delta = r^2 - 2Mr + a^2, \tag{3}$$

$$\Sigma^2 = (r^2 + a^2)^2 - a^2\Delta\sin^2\theta. \tag{4}$$

The inverse Kerr metric can be expressed as

$$[g^{\mu\nu}] = \begin{pmatrix} \frac{\Sigma^2}{\Delta\rho^2} & 0 & 0 & \frac{2Mar}{\Delta\rho^2} \\ 0 & -\frac{\Delta}{\rho^2} & 0 & 0 \\ 0 & 0 & -\frac{1}{\rho^2} & 0 \\ \frac{2Mar}{\Delta\rho^2} & 0 & 0 & -\frac{\Delta - a^2\sin^2\theta}{\rho^2\Delta\sin^2\theta} \end{pmatrix}, \tag{5}$$

which satisfies $g^{\mu\alpha}g_{\alpha\nu} = \delta^\mu_\nu$. The metric (1) is characterized by the black hole's mass M and angular momentum $J = Ma$. In this paper, we are only concerned with the range $r > r_+$, where $r_+ = M + \sqrt{M^2 - a^2}$ is the outer horizon.

The geodesic motion in Kerr spacetime can be written as decoupled, first-order equations:

$$\rho^2\dot{t} = \frac{1}{\Delta}(\Sigma^2 E - 2aMrL_z), \tag{6}$$

$$\rho^2\dot{\varphi} = \frac{1}{\Delta}(2aMrE + (\rho^2 - 2Mr)L_z\csc^2\theta), \tag{7}$$

$$\rho^4\dot{r}^2 \equiv R = E^2r^4 + (a^2E^2 - L_z^2 - D)r^2 - a^2D + 2Mr(D + (L_z - aE)^2) - m^2r\Delta, \tag{8}$$

$$\rho^4\dot{\theta}^2 \equiv \Theta = D + (a^2E^2 - L_z^2\csc^2\theta)\cos^2\theta - m^2a^2\cos^2\theta, \tag{9}$$

where a dot stands for a derivative with respect to the proper time s. These equations involve four constants of motion: the rest mass m, energy E, angular momentum L_z in the

z direction, and Carter constant D. The rest mass m is defined by

$$m^2 = g_{\mu\nu}\dot{x}^\mu \dot{x}^\nu. \tag{10}$$

Equations with $m = 0$ stand for null geodesics, and those with $m \neq 0$ stand for time-like geodesics. In this paper, we are only concerned with the case of $m \neq 0$. The energy E and z-axis angular momentum L_z are defined by

$$E = \left(1 - \frac{2Mr}{\rho^2}\right)\dot{t} + \frac{2Mar\sin^2\theta}{\rho^2}\dot{\varphi}, \tag{11}$$

$$L_z = -\frac{2Mar\sin^2\theta}{\rho^2}\dot{t} + \frac{\sin^2\theta}{\rho^2}\Sigma^2\dot{\varphi}. \tag{12}$$

The Carter constant D is defined by

$$D = \frac{1}{\Delta}(\Delta\dot{t} - a\Delta\sin^2\theta\dot{\varphi})^2 - \frac{\rho^4}{\Delta}\dot{r}^2 - m^2r^2 - (L_z - aE)^2. \tag{13}$$

Because the angular momentum L^2 is no longer a conserved quantity, the geodesic cannot travel in the same plane. This is the main difference between geodesic motion in a Kerr background and in a Schwarzschild background.

The Hamilton formulas can be used to describe the particle motion in Kerr spacetime. The Hamiltonian $H = \frac{1}{2}g_{\mu\nu}p^\mu p^\nu = \frac{m^2}{2}$ of geodesic motion is expressed as

$$H = \frac{1}{2}\left(\left(1 - \frac{2Mr}{\rho^2}\right)\dot{t}^2 + \frac{4Mar\sin^2\theta}{\rho^2}\dot{t}\,\dot{\varphi} - \frac{\rho^2}{\Delta}\dot{r}^2 - \rho^2\dot{\theta}^2 - \frac{\sin^2\theta}{\rho^2}\Sigma^2\dot{\varphi}^2\right). \tag{14}$$

The corresponding canonical momenta $(p_t, p_r, p_\theta, p_\varphi)$ can be calculated by

$$p_t = \frac{\partial H}{\partial \dot{t}} = E, \tag{15}$$

$$p_\varphi = -\frac{\partial H}{\partial \dot{\varphi}} = -L_z, \tag{16}$$

$$p_r = -\frac{\partial H}{\partial \dot{r}} = \frac{\rho^2}{\Delta}\dot{r} = \pm\frac{\sqrt{R}}{\Delta}, \tag{17}$$

$$p_\theta = -\frac{\partial H}{\partial \dot{\theta}} = \rho^2\dot{\theta} = \pm\sqrt{\Theta}. \tag{18}$$

Since the Hamiltonian does not contain t and φ, the Hamilton formulas show that E and L_z are constants, which are

$$\dot{p}_t = \frac{\partial H}{\partial t} = 0, \qquad \dot{p}_\varphi = \frac{\partial H}{\partial \varphi} = 0.$$

The symplectic variables (x^μ, p_μ) are understood as phase-space coordinates.

B. r motion

As $\rho^4\dot{r}^2 = R$, the function $\frac{R}{\rho^4}$ can be understood as the equivalent kinetic energy in the radial direction, whose properties are mainly determined by the function R. Simplifying Eq. (8), we obtain

$$R = (E^2 - m^2)r^4 + 2m^2Mr^3 + (a^2(E^2 - m^2) - L_z^2 - D)r^2 + 2M(D + (L_z - aE)^2)r - a^2D. \tag{19}$$

Particles in a Kerr background appear with non-negative kinetic energy, implying $R \geq 0$. Notice that R only depends on r and not on θ, therefore, the properties of r motion are independent of θ.

We consider the particles incident from infinity towards the black hole. The requirement that $R \geq 0 (r \to \infty)$ indicates that the energy satisfies $E \geq m$. Generally speaking, the function $R(r)$ has four zero points including both real and imaginary roots. For physical reasons, we only discuss positive real points. Let us define r_0 as the biggest real root of the equation $R = 0$. A test particle coming from infinity can travel to $r = r_0$. Once it arrives at $r = r_0$, its radial kinetic energy becomes zero. There exist three cases to discuss.

(1) $r_0 < r_+$: The test particle falls into the black hole.
(2) $r_0 > r_+$, and $R < 0$ for $r < r_0$: The test particle cannot enter the range $r < r_0$. It will be scattered by the black hole and travel to infinity. In this case, the position $r = r_0$ is the closest location, also known as the perihelion $r_p = r_0$.
(3) $r_0 > r_+$, and $R > 0$ for $r < r_0$: The test particle cannot travel to $r < r_0$, i.e., it keeps getting closer to $r = r_0$ but never reaches it. The position $r = r_0$ stands for an unstable orbit $r_c = r_0$.

Case 3 is a critical situation lying between case 1 and case 2. Since $R(r) > 0$ is true for both $r > r_0$ and $r < r_0$, $R(r_0) = 0$ is the minimum of the function $R(r)$. Then, case 3 satisfies

$$R(r_c, D_c) = 0, \tag{20}$$

$$\partial_r R(r_c, D_c) = 0. \tag{21}$$

The critical Carter constant parameter $D_c = D_c(E_{\min}, L_z, m)$ determines whether there is a perihelion along the geodesic motion, where $E_{\min}$ is the minimum energy possessed by a particle that can escape from the black hole. For geodesic motion with the parameter $D > D_c$, the perihelion exists and the particle should be scattered to infinity by the black hole; otherwise, the perihelion does not exist and the particle should be captured by the black hole. The numerical results are shown in Fig. 1.

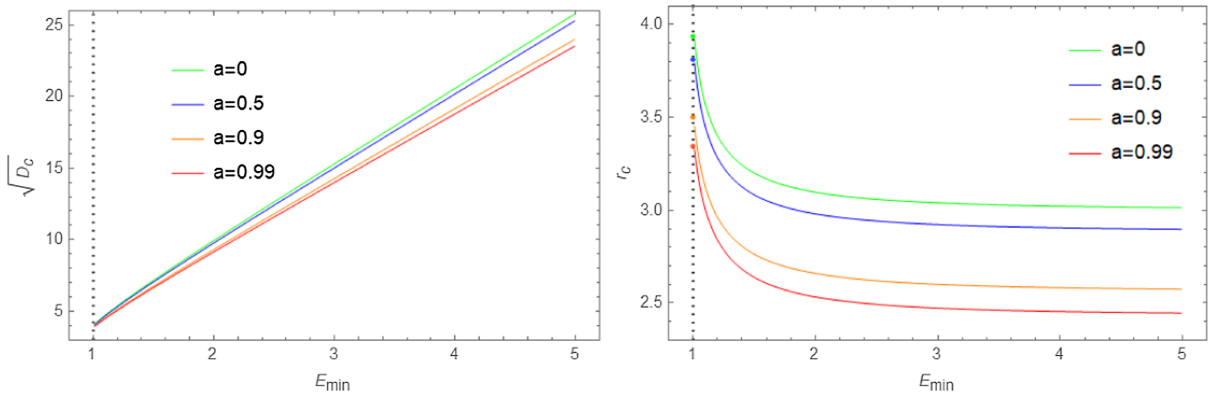

FIG. 1. Critical parameter $\sqrt{D_c}$ (left) and the unstable orbit r_c (right) as functions of the energy $E_{\min}$. Other parameters are chosen to be $M = 1$, $m = 0.01$, and $L_z = 0$.

The perihelion r_p only appears in the geodesic motion with the parameter $D > D_c$. Besides, the perihelion r_p lies in the range $r_p > r_c$.

C. θ motion

The behavior of θ motion is similar to that of r motion. As $\rho^4\dot{\theta}^2 = \Theta$, we take $\frac{\Theta}{\rho^4}$ as the equivalent kinetic energy in the θ direction, which is mainly influenced by the function $\Theta(\theta)$. Defining $y = \cos^2\theta \in [0, 1]$, one simplifies Eq. (9) to

$$\Theta = D + \left(a^2(E^2 - m^2) - \frac{L_z^2}{1-y}\right)y. \tag{22}$$

The root y_0 of $\Theta|_{y=y_0} = 0$ determines the range of θ in geodesic motion. We are only concerned with the physical situation where the zero point y_0 lies in $y_0 \in [0, 1]$. It is further divided into two cases.

(1) $L_z = 0$: One obtains

$$\Theta = D + a^2(E^2 - m^2)y, \tag{23}$$

which is monotonically increasing if $E > m$. For the parameter $D \geq 0$, the result $\Theta|_{y=0} \cdot \Theta|_{y=1} = D(D + a^2(E^2 - m^2)) > 0$ indicates that no zero points exist in the range [0, 1]. That is to say, the kinetic energy in the θ direction is always positive and the test particle can travel throughout the range of $\theta \in [0, \pi]$.

(2) $L_z \neq 0$: It can be proven that there is only one zero point in the interval [0, 1]. Denoting $y = y_0$ as the root, the particle can move in the range $\theta \in [\theta_0, \pi - \theta_0]$, where $\theta_0 = \arccos\sqrt{y_0} \in [0, \frac{\pi}{2}]$.

III. VLASOV GAS IN KERR GEOMETRY

A. Distribution function of Vlasov gas

A Vlasov gas is a collection of relativistic, free, and collisionless kinetic particles moving along geodesic lines. Unlike accretion onto a Schwarzschild black hole, accretion onto a Kerr black hole is no longer spherically symmetric, and considering the situation in only one plane is not enough. The distribution function $f(x^\mu, p_\mu)$ satisfies the collisionless Liouville equation

$$\dot{f} \equiv \{f, H\} = 0, \tag{24}$$

where the bracket $\{.,.\}$ stands for the Poisson bracket. The spherically symmetric solution of Eq. (24) has been discussed in detail in Ref. [12]. Similar to this, we seek the axisymmetric solution based on the transformation of symplectic variables $(x^\mu, p_\mu) \to (Q^\mu, P_\mu)$.

Following Carter's study [29], the abbreviated action S in Kerr geometry can be written as

$$S = \frac{1}{2}m^2\tau - Et + L_z\varphi + \int_r \frac{\sqrt{R}}{\Delta}dr + \int_\theta \sqrt{\Theta}d\theta, \tag{25}$$

where the integral bounds are the intervals of the geodesic motion. The new momenta P_μ are defined by the conserved quantities

$$P_0 = \sqrt{2H} = m, \tag{26}$$

$$P_1 = E, \tag{27}$$

$$P_2 = -L_z, \tag{28}$$

$$P_3 = \sqrt{D}. \tag{29}$$

The corresponding conjugate coordinates Q^μ are obtained as follows:

$$Q^0 = \frac{\partial S}{\partial m} = m\left(\tau - \int_r \frac{r^2}{\sqrt{R}}dr - \int_\theta \frac{a^2\cos^2\theta}{\sqrt{\Theta}}d\theta\right), \tag{30}$$

$$Q^1 = \frac{\partial S}{\partial E} = -t + \int_r \frac{Er^4 + a^2Er^2 - 2Mar(L_z - aE)}{\Delta\sqrt{R}}dr + \int_\theta \frac{a^2E\cos^2\theta}{\sqrt{\Theta}}d\theta, \tag{31}$$

$$Q^2 = \frac{\partial S}{\partial(-L_z)} = -\varphi + \int_r \frac{L_z r^2 - 2(L_z - aE)Mr}{\Delta\sqrt{R}}dr + \int_\theta \frac{L_z \cot^2\theta}{\sqrt{\Theta}}d\theta, \tag{32}$$

$$Q^3 = \frac{\partial S}{\partial\sqrt{D}} = \sqrt{D}\left(-\int_r \frac{1}{\sqrt{R}}dr + \int_\theta \frac{1}{\sqrt{\Theta}}d\theta\right). \tag{33}$$

The canonical transformations $(x^\mu, p_\mu) \to (Q^\mu, P_\mu)$ keep the Poisson bracket (24) covariant,

$$\frac{\partial H}{\partial p_\mu}\frac{\partial}{\partial x^\mu} - \frac{\partial H}{\partial x^\mu}\frac{\partial}{\partial p_\mu} = \frac{\partial H}{\partial P_\mu}\frac{\partial}{\partial Q^\mu} - \frac{\partial H}{\partial Q^\mu}\frac{\partial}{\partial P_\mu}. \tag{34}$$

In the new canonical variables (Q^μ, P_μ), the Hamiltonian becomes $H = \frac{P_0^2}{2}$. Therefore, the collisionless Liouville equation (24) is simplified to

$$\frac{\partial}{\partial Q^0} f = 0. \tag{35}$$

The general solution is given by

$$f = f(Q^1, Q^2, Q^3, P_0, P_1, P_2, P_3). \tag{36}$$

Besides, there exist more symmetry conditions to restrict the distribution function (24) from Kerr geometry. The Kerr metric is independent of t and φ which appear in Q^1 and Q^2. Then, the distribution function f can be simplified to a more simple form $f = f(Q^3, P_0, P_1, P_2, P_3)$. Moreover, as D is a constant, one has $\frac{\partial S}{\partial D} = 0$ [30] which further leads to $Q^3 = 0$. At last, it is indicated that the distribution function f in Kerr geometry depends only on the new momenta P_μ,

$$f = f(P_0, P_1, P_2, P_3). \tag{37}$$

B. Observable quantities

The observable quantities we are concerned with are the particle current density J_μ and the stress-energy-momentum tensor $T_{\mu\nu}$, which are defined at a spacetime point x of Kerr spacetime $\mathscr{M}$ by

$$J_\mu|_x = \int_\pi p_\mu f(x^\gamma, p_\gamma)\sqrt{-\det(g^{\alpha\beta})}d^4p, \tag{38}$$

$$T_{\mu\nu}|_x = \int_\pi p_\mu p_\nu f(x^\gamma, p_\gamma)\sqrt{-\det(g^{\alpha\beta})}d^4p, \tag{39}$$

where the integral range π is the subset of the cotangent space $T_x^*\mathscr{M}$, which will be determined according to the properties of the geodesic. Using Eq. (24), one can show that the particle current density J_μ and the energy-momentum tensor $T_{\mu\nu}$ satisfy the conservation laws

$$\nabla_\mu J^\mu = 0, \tag{40}$$

$$\nabla_\mu T^{\mu\nu} = 0. \tag{41}$$

The particle number density n_s is defined by J_μ through the relationship

$$n_s = \sqrt{g^{\mu\nu}J_\mu J_\nu}. \tag{42}$$

In the actual calculation, the momentum variables $(p_t, p_r, p_\theta, p_\varphi)$ transform to the variables (m^2, E, L_z, D), which can be reexpressed as follows:

$$m^2 = g^{00}p_t^2 + 2g^{03}p_t p_\varphi + g^{33}p_\varphi^2 + g^{11}p_r^2 + g^{22}p_\theta^2, \tag{43}$$

$$E = p_t, \tag{44}$$

$$K = \frac{(r^2+a^2)^2}{\Delta}p_t^2 + \frac{2a(a^2+r^2)}{\Delta}p_t p_\varphi + \frac{a^2}{\Delta}p_\varphi^2 - \Delta p_r^2 - m^2 r^2, \tag{45}$$

$$L_z = -p_\varphi. \tag{46}$$

Using the above equations, we obtain the Jacobian determinant

$$J = \frac{\partial(m^2, E, L_z, D)}{\partial(p_t, p_r, p_\theta, p_\varphi)} = \frac{4\sqrt{R\Theta}}{\rho^2}, \tag{47}$$

and simplify the volume element as

$$\sqrt{-\det(g^{\mu\nu})}dp_t dp_r dp_\theta dp_\varphi = \frac{dm^2 dE dL_z dD}{4\sqrt{R\Theta}\sin\theta}. \tag{48}$$

Next, we further simplify the volume element in two different cases.

(1) Nonequatorial plane $\theta \neq \frac{\pi}{2}$:

In a nonequatorial plane $\theta \neq \frac{\pi}{2}$, there exist constraints on L_z to ensure that $\Theta > 0$. Let us define

$$X^2 = \tau\sin^2\theta + (E^2 - m^2)a^2\sin^2\theta, \tag{49}$$

$$\tau = \frac{D}{\cos^2\theta}. \tag{50}$$

Inserting these expressions into Eq. (9), one obtains

$$\Theta\sin^2\theta = \cos^2\theta(X^2 - L_z^2). \tag{51}$$

Thus, the integral range of L_z is $L_z \in [-X, X]$. Furthermore, we make the substitution

$$L_z = X\sin\sigma \tag{52}$$

and obtain

$$\frac{dL_z}{\sqrt{\Theta \sin^2\theta}} = \frac{d\sigma}{|\cos\theta|}. \tag{53}$$

The integral range of σ is $\sigma \in [-\frac{\pi}{2}, \frac{\pi}{2}]$. At last, the volume element is reexpressed as

$$\sqrt{-\det(g^{\mu\nu})}dp_t dp_r dp_\theta dp_\varphi = \frac{|\cos\theta|}{4\sqrt{R}} dm^2 dE d\tau d\sigma. \tag{54}$$

Notice that the definition (50) becomes divergent when $\theta = \pi/2$, and thus the above expression for the volume element is not applicable to the case of the equatorial plane. Therefore, for the case of $\theta = \pi/2$ we have to do the calculations separately.

(2) Equatorial plane $\theta = \frac{\pi}{2}$:

In the equatorial plane $\theta = \frac{\pi}{2}$, Θ degenerates to D. There is no constraint on L_z. The integral range of L_z is simply $L_z \in (-\infty, \infty)$ and the volume element is expressed as

$$\sqrt{-\det(g^{\mu\nu})}dp_t dp_r dp_\theta dp_\varphi = \frac{dm^2 dE dL_z dD}{4\sqrt{D}\sqrt{R}}. \tag{55}$$

In Sec. II, the geodesic motion coming from infinity, also named the unbounded orbit and satisfying $E > m$, was divided into three classifications. The key of the classification is based on the values of the parameters (m^2, E, L_z, D) or, equivalently, the parameters (m^2, E, σ, τ). For particles absorbed by the black hole, there is no perihelion along their trajectories, which indicates that the parameter τ lies in the range $\tau < \tau_c$. For particles scattered by the black hole, the perihelion r_p exits and the parameter τ is in the range $\tau > \tau_c$. In the critical case between them, particles are neither absorbed nor scattered by the black hole, but get infinitely close to the unstable orbit r_c. In this case, the value of the parameter τ is $\tau = \tau_c$. According to the classification of the orbit, the observable quantity J_μ or $T_{\mu\nu}$ consists of three parts: the absorbed part, the scattered part, and the critical part. That is,

$$J_\mu = J_\mu^{\text{abs}} + J_\mu^{\text{scat}} + J_\mu^{\text{cri}}, \tag{56}$$

$$T_{\mu\nu} = T_{\mu\nu}^{\text{abs}} + T_{\mu\nu}^{\text{scat}} + T_{\mu\nu}^{\text{cri}}, \tag{57}$$

where the critical part does not have a substantial contribution and attracts no attention in most cases. Notice that the observable quantities (38) and (39) depend on both r and θ. If the distribution function $f(x^\mu, p_\mu)$ is given, J_μ and $T_{\mu\nu}$ can be calculated.

C. Accretion rates

Because the geodesic motion is not in a single plane, the collisionless particles are no longer in a single plane, too. We suppose that they are distributed throughout all of the space outside the black hole. Since the flow is stationary and axisymmetric, the equation $\nabla_\mu J^\mu = 0$ becomes

$$(\rho^2 \sin\theta J^r)_{,r} + (\rho^2 \sin\theta J^\theta)_{,\theta} = 0. \tag{58}$$

Let V be a region in Kerr spacetime and S be a 2-surface boundary of V. The above equation shows that the integral of the left side in V is a constant, which is called the mass accretion rate. Consider that a vector $\hat{n} = (n_r, n_\theta, 0)$ is the unit normal field of S that is directed outside. Using Stokes' theorem, the mass accretion rate is expressed as

$$\frac{dM}{dt} = -\int_V ((\rho^2 \sin\theta J^r)_{,r} + (\rho^2 \sin\theta J^\theta)_{,\theta}) dV, \tag{59}$$

$$= -\int_S (J^r \hat{n}_r + J^\theta \hat{n}_\theta)\rho^2 d\Omega, \tag{60}$$

where $d\Omega = \sin\theta d\theta d\varphi$ and the current flux J^μ traverses through S. On the other hand, $T_{\mu\nu}$ are also divergence free, so there exist two more accretion rates besides the mass accretion rate in Kerr geometry. They are the energy and angular momentum accretion rates and are expressed as follows:

$$\frac{d\mathcal{E}}{dt} = -\int_S (T^r{}_t \hat{n}_r + T^\theta{}_t \hat{n}_\theta)\rho^2 d\Omega, \tag{61}$$

$$\frac{d\mathcal{L}}{dt} = -\int_S (T^r{}_\varphi \hat{n}_r + T^\theta{}_\varphi \hat{n}_\theta)\rho^2 d\Omega. \tag{62}$$

As considered by other authors, we are only concerned with the fact that the 2-surface S is a spherical surface with the surface element $dS = r^2 d\Omega$, where the unit external normal vector is chosen as $\hat{n} = (1, 0, 0)$. The corresponding accretion rates through a unit surface are expressed as

$$\frac{d^2M}{dSdt} = J_r \frac{\Delta}{r^2}, \tag{63}$$

$$\frac{d^2\mathcal{E}}{dSdt} = T_{rt} \frac{\Delta}{r^2}, \tag{64}$$

$$\frac{d^2\mathcal{L}}{dSdt} = T_{r\varphi} \frac{\Delta}{r^2}. \tag{65}$$

IV. EXPLICIT EXAMPLE AND LIMITS OF INTEGRATION

We consider a stationary, axially symmetric, collisionless gas distributed throughout all of the Kerr spacetime. Notice that it is no longer a disk confined to a constant θ_0 plane.

At infinity, the Kerr metric is asymptotically flat and we suppose that the gas satisfies the same asymptotic condition as in a spherically symmetric spacetime. As an explicit example, we choose the distribution function

$$f = \delta(P_0 - m_0) f_\infty(P_1)|_{P_1=E} = A\delta(P_0 - m_0)e^{-\beta P_1}, \tag{66}$$

where m_0 is the mass of the particles and A is the normalization factor. The variable $\beta = \frac{1}{k_b T}$, where k_b is the Boltzmann constant and T is the asymptotic temperature. The distribution function (66) fulfills the conclusion (37) of a Vlasov gas in Kerr geometry.

A. Nonequatorial plane $\theta \neq \frac{\pi}{2}$

Using dimensionless variables, we redefine

$$E = m_0\varepsilon, \tag{67}$$

$$\tau = m_0^2\bar{\tau}, \tag{68}$$

$$X^2 = m_0^2\bar{X}^2, \tag{69}$$

$$R = m_0^2\bar{R}, \tag{70}$$

where X is expressed as in Eq. (49) and R is expressed as in Eq. (19). Therefore, we have

$$\bar{X}^2 = (\bar{\tau} + (\varepsilon^2 - 1)a^2)\sin^2\theta, \tag{71}$$

$$\Theta = m_0^2\bar{X}^2\cos^2\sigma\frac{\cos^2\theta}{\sin^2\theta}, \tag{72}$$

$$\bar{R} = (\varepsilon^2 - 1)r^4 + 2Mr^3 + (a^2(\varepsilon^2 - 1) - \bar{X}^2\sin^2\sigma - \bar{\tau}\cos^2\theta)r^2 + 2M(\bar{\tau}\cos^2\theta + (\bar{X}\sin\sigma - a\varepsilon)^2)r - a^2\bar{\tau}\cos^2\theta. \tag{73}$$

Next, we discuss the upper and lower limits of the integral element corresponding to the absorption part and the scattering part.

We solve the simultaneous equations

$$\partial_r\bar{R} = 0, \tag{74}$$

$$\bar{R} = 0, \tag{75}$$

and obtain the solutions

$$r = r_c(\varepsilon, \sigma; \theta), \tag{76}$$

$$\bar{\tau} = \bar{\tau}_c(\varepsilon, \sigma; \theta). \tag{77}$$

For the absorption part, as we have stated, there is no perihelion on these geodesic orbits. Thus, the interval of the element $\bar{\tau}$ is in the range $\bar{\tau} \in [0, \bar{\tau}_c]$. From Eq. (72), Θ is always positive, and no additional conditions are provided for constraining σ from Θ. So the range of σ is $\sigma \in [-\frac{\pi}{2}, \frac{\pi}{2}]$. The limits of the element ε are related to the energy condition of the Vlasov gas. In this paper, we are only concerned with the fact that the black hole accretes particles traveling from infinity and the parameter ε satisfies $\varepsilon \in [1, \infty)$. Plugging the distribution function (66) into the observable quantities (38) and (39), we obtain the absorption part as follows:

$$J_t^{\text{abs}}(r,\theta) = Am_0^4\int_{-\frac{\pi}{2}}^{\frac{\pi}{2}} d\sigma \int_1^\infty d\varepsilon \int_0^{\bar{\tau}_c} d\bar{\tau}\frac{\varepsilon e^{-\bar{\beta}\varepsilon}|\cos\theta|}{2\sqrt{\bar{R}}}, \tag{78}$$

$$J_r^{\text{abs}}(r,\theta) = Am_0^4\int_{-\frac{\pi}{2}}^{\frac{\pi}{2}} d\sigma \int_1^\infty d\varepsilon \int_0^{\bar{\tau}_c} d\bar{\tau}\frac{e^{-\bar{\beta}\varepsilon}|\cos\theta|}{2\Delta}, \tag{79}$$

$$J_\theta^{\text{abs}}(r,\theta) = Am_0^4\int_{-\frac{\pi}{2}}^{\frac{\pi}{2}} d\sigma \int_1^\infty d\varepsilon \int_0^{\bar{\tau}_c} d\bar{\tau}\frac{\bar{X}e^{-\bar{\beta}\varepsilon}\cos\sigma\cos^2\theta}{2\sqrt{\bar{R}}\sin\theta}, \tag{80}$$

$$J_\varphi^{\text{abs}}(r,\theta) = -Am_0^4\int_{-\frac{\pi}{2}}^{\frac{\pi}{2}} d\sigma \int_1^\infty d\varepsilon \int_0^{\bar{\tau}_c} d\bar{\tau}\frac{\bar{X}e^{-\bar{\beta}\varepsilon}\sin\sigma|\cos\theta|}{2\sqrt{\bar{R}}}, \tag{81}$$

where $\bar{\beta} = m_0\beta$. Notice that $T_{\mu\nu}$ have ten components and we list them in the Appendix.

By evaluating the integrals through new coordinates $x = \sqrt{\varepsilon^2 - 1}\sin\sigma$, $y = \sqrt{\varepsilon^2 - 1}\cos\sigma$, and $z = \frac{\bar{\tau}}{\varepsilon^2 - 1}$, we can prove that $J_\theta = 0, T_{r\theta} = 0, T_{\theta\phi} = 0, T_{t\theta} = 0$ and $J_\phi \neq 0, T_{t\phi} \neq 0$. Since we consider the fluid passing through a 2-sphere, and as is shown in Eq. (58), the accretion rates are defined by two Killing vectors ∂_t and ∂_ϕ. Thus, J^ϕ and $T^t{}_\phi$ would not appear in the accretion rates. On the other hand, to compare with the accretion of an isotropic perfect fluid is also an interesting topic [13] but it is not within the scope of this paper. We will do a more detailed study in the future to compare our model with the accretion of a perfect fluid.

For the scattering part, the range of σ is also simply in $\sigma \in [-\frac{\pi}{2}, \frac{\pi}{2}]$. Particles with energy $\varepsilon > 1$ can escape from the black hole at a close position r_c, which is determined by Eqs. (74) and (75), and also illustrated in Fig. 1. For scattering particles, the radial coordinate is divided into two segments according to whether $r \geq r_{c1}$, where r_{c1} is determined by $\partial_r\bar{R}|_{\varepsilon=1} = 0, \bar{R}|_{\varepsilon=1} = 0$; see the intersection point of the r_c curve with the $E_{\text{min}} = 1$ line in Fig. 1. In the range $r \geq r_{c1}$, the lower energy of scattering particles is $\varepsilon_{\text{min}} = 1$. For those particles that can escape from the black hole in the range $r < r_{c1}$, they must have energy $\varepsilon > \varepsilon_{\text{min}} > 1$. When performing the actual calculation, we use the FindRoot command to obtain the inverse function $r_c(E_{\text{min}})$ appearing in Fig. 1. Therefore, the lower limit of ε is

$$\varepsilon_{\min} = \begin{cases} \varepsilon(r), & r < r_{c1}, \\ 1, & r \geq r_{c1}. \end{cases} \tag{82}$$

The upper limit of ε is still infinity. For the limits of τ, the scattering part must have a perihelion, and thus $\tau > \tau_c$. At the same time, the signature of the function R must be positive. Solving $\bar{R} = 0$, one obtains $\bar{\tau} = \bar{\tau}_{\max}$. Notice that $\bar{\tau}_{\max}$ depends on both ε and σ. Thus, the range of $\bar{\tau}$ satisfies $\bar{\tau}_c > \bar{\tau} > \bar{\tau}_{\max}$. In addition, we have to note that the trajectory of the scattering part contains both $+\sqrt{R}$ and $-\sqrt{R}$, and thus

$$J_t^{\text{scat}}(r,\theta) = Am_0^4 \sum_{\pm} \int_{-\frac{\pi}{2}}^{\frac{\pi}{2}} d\sigma \int_{\varepsilon_{\min}}^{\infty} d\varepsilon \int_{\bar{\tau}_c}^{\bar{\tau}_{\max}} d\bar{\tau} \frac{\varepsilon e^{-\bar{\beta}\varepsilon} |\cos\theta|}{2\sqrt{\bar{R}}}, \tag{83}$$

$$J_r^{\text{scat}}(r,\theta) = Am_0^4 \sum_{\pm} \int_{-\frac{\pi}{2}}^{\frac{\pi}{2}} d\sigma \int_{\varepsilon_{\min}}^{\infty} d\varepsilon \int_{\bar{\tau}_c}^{\bar{\tau}_{\max}} d\bar{\tau} \frac{e^{-\bar{\beta}\varepsilon} |\cos\theta|}{2\Delta}, \tag{84}$$

$$J_\theta^{\text{scat}}(r,\theta) = Am_0^4 \sum_{\pm} \int_{-\frac{\pi}{2}}^{\frac{\pi}{2}} d\sigma \int_{\varepsilon_{\min}}^{\infty} d\varepsilon \int_{\bar{\tau}_c}^{\bar{\tau}_{\max}} d\bar{\tau} \times \frac{\bar{X} e^{-\bar{\beta}\varepsilon} \cos\sigma \cos^2\theta}{2\sqrt{\bar{R}} \sin\theta}, \tag{85}$$

$$J_\varphi^{\text{scat}}(r,\theta) = -Am_0^4 \sum_{\pm} \int_{-\frac{\pi}{2}}^{\frac{\pi}{2}} d\sigma \int_{\varepsilon_{\min}}^{\infty} d\varepsilon \int_{\bar{\tau}_c}^{\bar{\tau}_{\max}} d\bar{\tau} \times \frac{\bar{X} e^{-\bar{\beta}\varepsilon} \sin\sigma |\cos\theta|}{2\sqrt{\bar{R}}}. \tag{86}$$

B. Equatorial plane $\theta = \frac{\pi}{2}$

The calculation in the equatorial plane is very similar to that in a nonequatorial plane. We define

$$L_z = m_0 l_z, \tag{87}$$

$$D = m_0^2 \xi, \tag{88}$$

and

$$\bar{R}_0 = (\varepsilon^2 - 1) r^4 + 2Mr^3 + (a^2(\varepsilon^2 - 1) - l_z^2 - \xi) r^2 + 2M(\xi + (l_z - a\varepsilon)^2) r - a^2 \xi, \tag{89}$$

where $R = m_0 \bar{R}_0$. J_μ in the absorption part are expressed as

$$J_t^{\text{abs}}\left(r, \frac{\pi}{2}\right) = Am_0^4 \int_{-\infty}^{\infty} dl_z \int_1^{\infty} d\varepsilon \int_0^{\xi_c} d\xi \frac{\varepsilon e^{-\bar{\beta}\varepsilon}}{2\sqrt{\xi}\sqrt{\bar{R}_0}}, \tag{90}$$

$$J_r^{\text{abs}}\left(r, \frac{\pi}{2}\right) = Am_0^4 \int_{-\infty}^{\infty} dl_z \int_1^{\infty} d\varepsilon \int_0^{\xi_c} d\xi \frac{e^{-\bar{\beta}\varepsilon}}{2\Delta\sqrt{\xi}}, \tag{91}$$

$$J_\theta^{\text{abs}}\left(r, \frac{\pi}{2}\right) = Am_0^4 \int_{-\infty}^{\infty} dl_z \int_1^{\infty} d\varepsilon \int_0^{\xi_c} d\xi \frac{e^{-\bar{\beta}\varepsilon}}{2\sqrt{\bar{R}_0}}, \tag{92}$$

$$J_\varphi^{\text{abs}}\left(r, \frac{\pi}{2}\right) = -Am_0^4 \int_{-\infty}^{\infty} dl_z \int_1^{\infty} d\varepsilon \int_0^{\xi_c} d\xi \frac{l_z e^{-\bar{\beta}\varepsilon}}{2\sqrt{\xi}\sqrt{\bar{R}_0}}, \tag{93}$$

and in the scattering part they are expressed as

$$J_t^{\text{scat}}\left(r, \frac{\pi}{2}\right) = Am_0^4 \sum_{\pm} \int_{-\infty}^{\infty} dl_z \int_{\varepsilon_{\min}}^{\infty} d\varepsilon \int_{\xi_c}^{\xi_{\max}} d\xi \frac{\varepsilon e^{-\bar{\beta}\varepsilon}}{2\sqrt{\xi}\sqrt{\bar{R}_0}}, \tag{94}$$

$$J_r^{\text{scat}}\left(r, \frac{\pi}{2}\right) = Am_0^4 \sum_{\pm} \int_{-\infty}^{\infty} dl_z \int_{\varepsilon_{\min}}^{\infty} d\varepsilon \int_{\xi_c}^{\xi_{\max}} d\xi \frac{e^{-\bar{\beta}\varepsilon}}{2\Delta\sqrt{\xi}}, \tag{95}$$

$$J_\theta^{\text{scat}}\left(r, \frac{\pi}{2}\right) = Am_0^4 \sum_{\pm} \int_{-\infty}^{\infty} dl_z \int_{\varepsilon_{\min}}^{\infty} d\varepsilon \int_{\xi_c}^{\xi_{\max}} d\xi \frac{e^{-\bar{\beta}\varepsilon}}{2\sqrt{\bar{R}_0}}, \tag{96}$$

$$J_\varphi^{\text{scat}}\left(r, \frac{\pi}{2}\right) = -Am_0^4 \sum_{\pm} \int_{-\infty}^{\infty} dl_z \int_{\varepsilon_{\min}}^{\infty} d\varepsilon \int_{\xi_c}^{\xi_{\max}} d\xi \frac{l_z e^{-\bar{\beta}\varepsilon}}{2\sqrt{\xi}\sqrt{\bar{R}_0}}. \tag{97}$$

In fact, the values of $J_\mu(r,\theta)$ and $T_{\mu\nu}(r,\theta)$ are continuous as θ increases from $\theta = 0$ to $\theta = \frac{\pi}{2}$.

V. ASYMPTOTIC BEHAVIOR

Before doing the numerical computation, we analytically discuss the asymptotic behavior of $J_\mu(r,\theta)$ and $T_{\mu\nu}(r,\theta)$. By using Taylor series, the asymptotic behavior can be calculated at large distance. For brevity, we simply define $Am_0^4 = Am_0^5 = 1$ and choose $\bar{\beta} = 1$.

Far away from the black hole, the absorption part becomes zero and only contributions of the scattering part remain. Using a Taylor expansion of $\frac{1}{r}$, the function $\frac{1}{\sqrt{\bar{R}}}$ is expressed as

$$\frac{1}{\sqrt{\bar{R}}} = \frac{1}{\sqrt{\varepsilon^2 - 1}} \left(\frac{1}{r^2} - \frac{M}{(\varepsilon^2 - 1) r^3} \right), \tag{98}$$

where only the first two terms are listed. Since the integrand is independent of $\bar{\tau}$, the integral with respect to $\bar{\tau}$ is simply

$$\int_{\bar{\tau}_c}^{\bar{\tau}_{\max}} d\bar{\tau} = \bar{\tau}_{\max} - \bar{\tau}_c, \tag{99}$$

where $\bar{\tau}_c$ does not depend on r. Since $\bar{\tau}_{\max}$ is determined by $\bar{R} = 0$, it is expressed as

$$\bar{\tau}_{\max} = \frac{r^2}{\cos^2\theta + \sin^2\theta \sin^2\sigma}\left((\varepsilon^2-1) + 2M\varepsilon^2\frac{1}{r}\right) \quad (100)$$

using a Taylor expansion. The direct calculation of Eq. (83) gives

$$J_t(r\to\infty) = \int_{-\frac{\pi}{2}}^{\frac{\pi}{2}} d\sigma \int_1^\infty d\varepsilon \frac{\bar{\tau}_{\max}}{\sqrt{\bar{R}}} \varepsilon e^{-\varepsilon} |\cos\theta|$$
$$= \pi\left(K_2(1) + (2K_0(1) + 5K_1(1))\frac{M}{r}\right), \quad (101)$$

where $K_n(x)$ is the second Bessel function. The values of $K_n(x)$ can be found in the related books. Thus, the above expression approximates to

$$J_t(r\to\infty) = 5.104 + 12.100\frac{M}{r}, \quad (102)$$

which agrees with the numerical computation in the next section. Notice that the expression for J_t is independent of θ at infinity. If $\bar{\beta}$ is an arbitrary constant, the first term of $J_t(r\to\infty)$ is

$$J_t(r\to\infty) = \frac{\pi K_2(\bar{\beta})}{\bar{\beta}}. \quad (103)$$

Thus, the particle density n_∞ at infinity is

$$n_\infty = \pi\frac{K_2(\bar{\beta})}{\bar{\beta}}. \quad (104)$$

This result is proportional to that in Ref. [12]; see also Appendix B in Ref. [27]. The difference can be eliminated by choosing the normalized constant A appropriately.

Similar to the calculation of $J_t(r\to\infty)$, the values of other components at infinity can be calculated as follows:

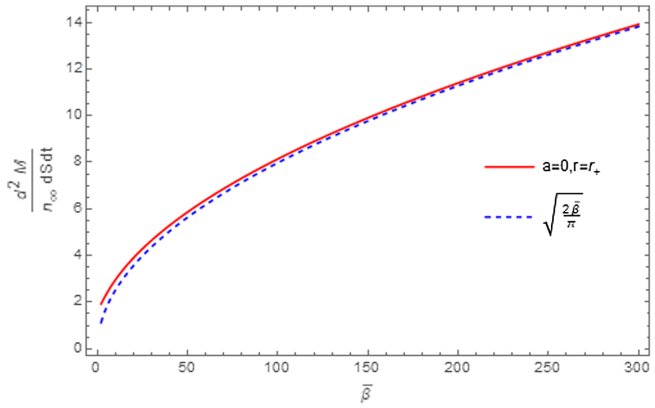

FIG. 2. Asymptotic behavior of the unit mass accretion rate in the low-temperature limit. As $\bar{\beta}$ increases, the unit mass accretion rate coincides with the function $\sqrt{\frac{2\bar{\beta}}{\pi}}$.

$$J_r(r\to\infty) = \frac{4\pi}{e} + \frac{18\pi}{e}\frac{M}{r}, \quad (105)$$

$$T_{tr}(r\to\infty) = \frac{14\pi}{e} + \frac{60\pi}{e}\frac{M}{r}, \quad (106)$$

$$T_{r\varphi}(r\to\infty) = 0. \quad (107)$$

At large distance, the Kerr metric can be approximated as the Schwarzschild one and the parameter a has no effect. This is the main reason that J_μ and $T_{\mu\nu}$ are independent of θ at infinity.

Our results can be approximated by the Schwarzschild case in the low-temperature limit. The process is as follows. Near the horizon r_+, the scattering part is omitted. In the special case $a = 0$, the background spacetime is approximated by the Schwarzschild metric. The critical value of $\bar{\tau}_c$ can be calculated as

$$\bar{\tau}_c = \frac{M^2(9(3\epsilon^2 + \sqrt{\epsilon^2(9\epsilon^2-8)} - 4)\epsilon^2 - 8\sqrt{\epsilon^2(9\epsilon^2-8)} + 8)}{2(\epsilon^2-1)(\sin^2\theta\sin^2\sigma + \cos^2\theta)}. \quad (108)$$

We notice that as $r\to r_+$, $\Delta(r_+)$ turns into 0 and J_r becomes infinity. However, the unit accretion mass $\frac{d^2M}{dSdt}$ is a finite value. We obtain

$$\left.\frac{d^2M}{n_\infty dSdt}\right|_{r_+} = \frac{\bar{\beta}}{16K_2(\bar{\beta})}\int_1^\infty \frac{9(3\epsilon^2 + \sqrt{\epsilon^2(9\epsilon^2-8)} - 4)\epsilon^2 - 8\sqrt{\epsilon^2(9\epsilon^2-8)} + 8}{(\epsilon^2-1)} e^{-\bar{\beta}\epsilon} d\epsilon. \quad (109)$$

In the low-temperature limit $\bar{\beta}\to\infty$, Ref. [12] gave a result for mass accretion rate,

$$\left.\frac{1}{n_\infty}\frac{dM}{dt}\right|_{\text{low}} = 16\sqrt{2\pi}M^2\sqrt{\bar{\beta}}, \quad (110)$$

where, compared to Ref. [12], the difference is just due to the normalization we chose, $m_0 = 1$. Considering the area of the horizon surface $S = 4\pi r_+^2 = 16\pi M^2$, we have

$$\left.\frac{d^2M}{n_\infty dSdt}\right|_{\text{low}} = \sqrt{\frac{2\bar{\beta}}{\pi}}. \tag{111}$$

The numerical calculation shows that Eqs. (109) and (111) coincide with each other as $\bar{\beta}$ increases; see Fig. 2.

VI. NUMERICAL RESULTS

In doing the numerical computation, without loss of generality, we choose $M = \bar{\beta} = m_0 = A = 1$. Similar to Fig. 1, the numerical relationship between ε and r_c is plotted in Fig. 3. In the calculation of the scattering part, the function $\varepsilon(r_c)$ determines the lower integral bound of ε. The common method is to find the inverse function of $r_c(\varepsilon)$ through FindRoot.

The variations of J_t with r are plotted in Fig. 4, which shows that with increasing r, the absorption part is monotonically decreasing, and the scattering part and the total are monotonically increasing. J_r, T_{tr}, and $T_{\varphi r}$ have similar behaviors shown in Figs. 5–7, respectively.

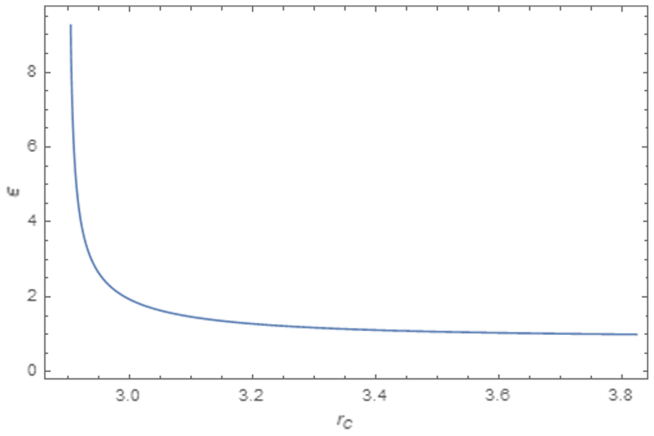

FIG. 3. Numerical relationship between ε and r_c. The minimum value of r_c approaches the photon sphere of the Kerr black hole. The parameters are chosen to be $\theta = \frac{\pi}{3}, \sigma = \frac{\pi}{3}, a = 0.1$.

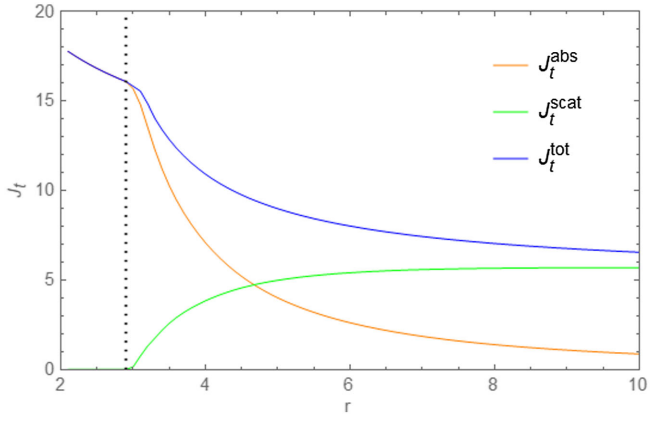

FIG. 4. J_t as a function of r. The parameters are chosen to be $\theta = \frac{\pi}{3}, a = 0.1$. The upper integral bound of ε is truncated to $\varepsilon = 8$. The dotted line stands for the photon sphere $r = r_{\text{ph}}$. In the range $r < r_{\text{ph}}$, there are no scattered particles.

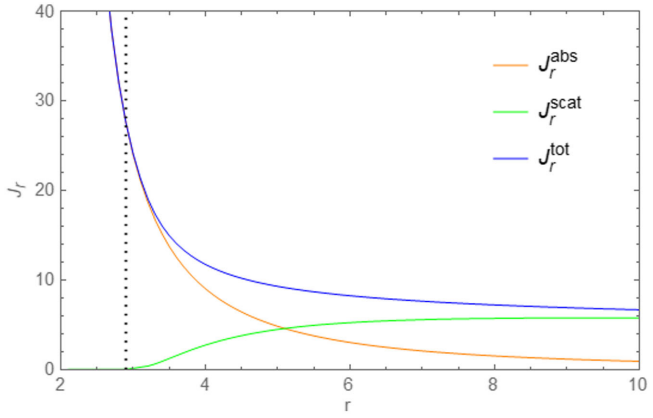

FIG. 5. J_r as a function of r. The parameters are chosen to be $\theta = \frac{\pi}{3}, a = 0.1$.

We also consider the variations of the particle current densities and the stress-energy-momentum with respect to θ at the horizon. Since J_r, T_{tr}, and $T_{\varphi r}$ approach infinity at the horizon, we plot $J_t|_{r_+}$ as a function of θ in Fig. 8. It is shown that $J_t|_{r_+}$ increases slightly when θ changes from 0 to $\frac{\pi}{2}$.

Furthermore, the unit accretion rates of the black hole are very relevant in physics. In this paper, we are concerned with the accretion rates changing with θ at the horizon. We plot the unit mass accretion rate $\frac{d^2M}{n_\infty dSdt}|_{r_+}$ as a function of θ in Fig. 9, which shows a weak growth as θ approaches the equatorial plane. A similar behavior also appears in the energy accretion rate $\frac{d^2\mathcal{E}}{n_\infty dSdt}|_{r_+}$; see Fig. 10. However, as seen in Fig. 11, the unit momentum accretion rate grows more rapidly as θ increases. These behaviors imply that the unit accretion rates at the horizon surface have different growth trends. As the accretion goes on, the background

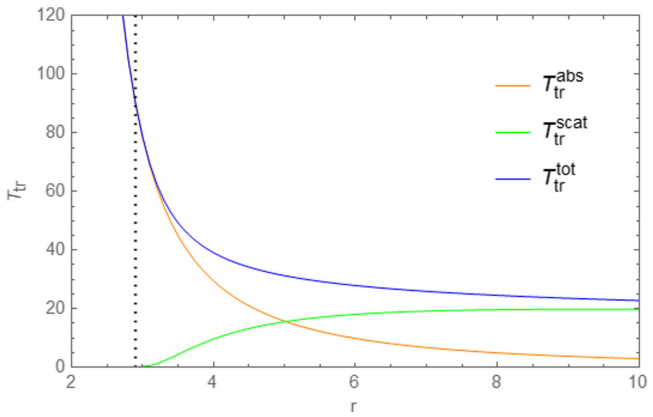

FIG. 6. T_{tr} as a function of r. The parameters are chosen to be $\theta = \frac{\pi}{3}, a = 0.1$.

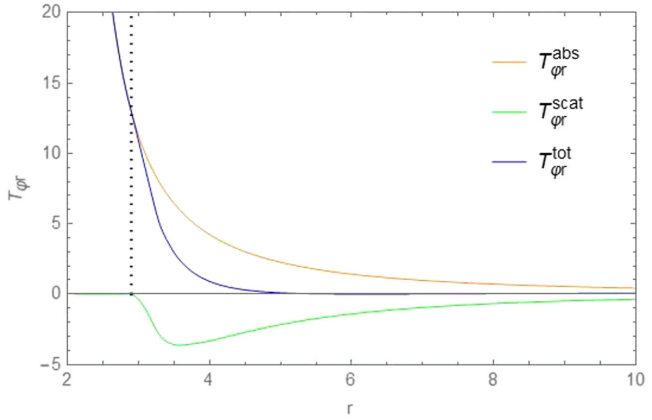

FIG. 7. $T_{\varphi r}$ as a function of r. The parameters are chosen to be $\theta = \frac{\pi}{3}, a = 0.1$.

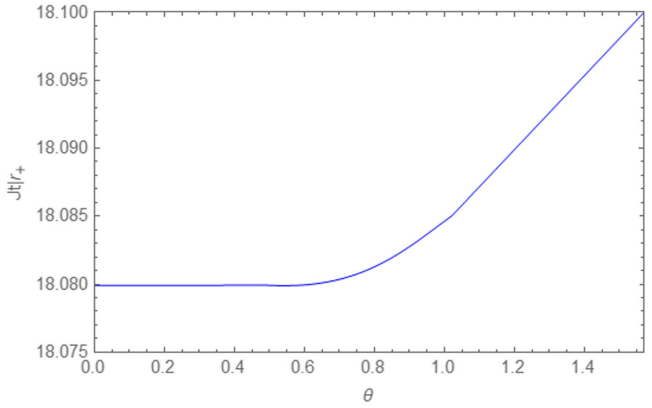

FIG. 8. $J_t|_{r_+}$ as a function of θ. The parameter is chosen to be $a = 0.1$. It increases slightly when θ changes from 0 to $\frac{\pi}{2}$.

would deviate from the Kerr one, depending on the total mass of particles falling into the black hole. Figure 9 also shows that the unit mass accretion rate increases nonlinearly as a grows, which would further alleviate the BHL

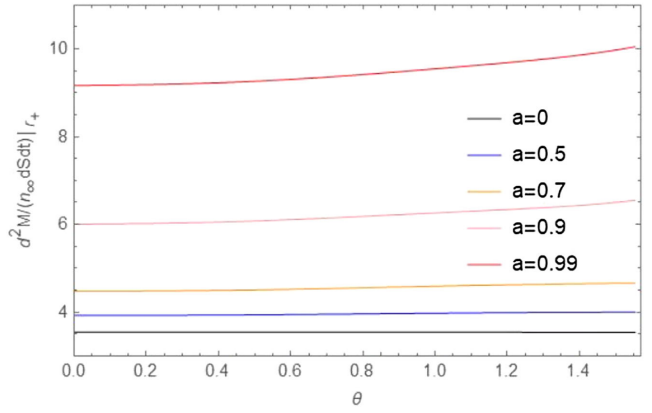

FIG. 9. Unit mass accretion rate $\frac{d^2M}{n_\infty dSdt}|_{r_+}$ as a function of θ. The range of θ is throughout the northern hemisphere $\theta \in [0, \frac{\pi}{2}]$. The behavior in the southern hemisphere is symmetric to that in the northern hemisphere.

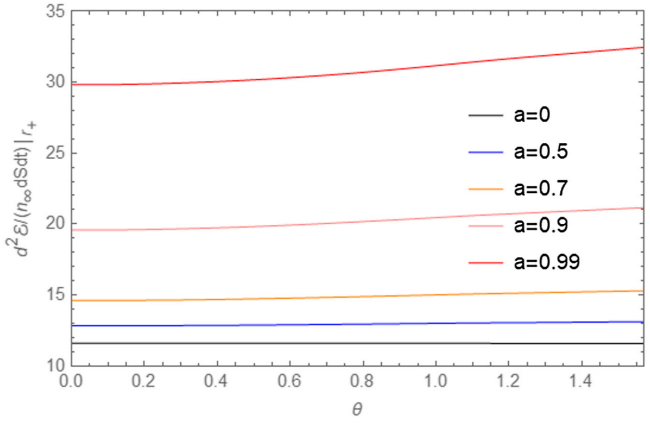

FIG. 10. Unit energy accretion rate $\frac{d^2\mathcal{E}}{n_\infty dSdt}|_{r_+}$ as a function of θ.

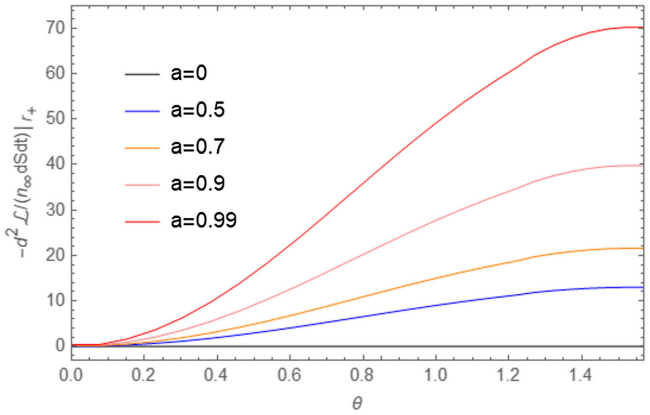

FIG. 11. Unit angular momentum accretion rate $-\frac{d^2\mathcal{L}}{n_\infty dSdt}|_{r_+}$ as a function of θ.

accretion problem. From Fig. 11, we also know that for larger a, the black hole is slowed down more quickly by accretion.

VII. CONCLUSION

In this paper, we studied the accretion of Vlasov gas onto a Kerr black hole, where particles are distributed throughout all of the spacetime. The main conclusions are as follows.

We solved the relativistic Liouville equation in the Kerr background. We proved that the distribution function is independent of Q^μ if the flow is stationary and axisymmetric.

We derived the expression of the volume element corresponding to the equatorial plane and nonequatorial plane. We also obtained the expressions of three unit accretion rates surrounded by a sphere.

In an example of a Maxwell-Jüttner distribution at infinity, we further calculated the particle current density J_μ, stress-energy-momentum tensor $T_{\mu\nu}$, and three unit accretion rates. At large distance, we first gave a convenient analytical computing method, which shows that all quantities are independent on θ, and the correlative results are

approximated by those in the Schwarzschild case. In the nonrotating case $a \to 0$, the unit mass accretion rate is computed by numerical methods and is coincident to the result in the Schwarzschild case. In the finite range, the corresponding calculation results were obtained by numerical methods.

The numerical results show growths of the accretion rates as θ approaches the equatorial plane. If the mass of particles falling into the black hole is much less than the mass of the black hole, that is, $m_{\rm gas} \ll M$, the background metric remains unchanged. However, as the Vlasov particles keep flowing into the black hole, $m_{\rm gas}$ increases continuously, and the background metric may change inevitably.

The numerical results also show nonlinear growth of the accretion rates as a approaches M, which implies the possibility of alleviating the BHL accretion problem if the black hole is rotating.

As is known, a realistic accretion flow will involve magnetic fields, which will mediate the effective collisionality between the particles. To consider the effect of magnetic fields will be an interesting topic worth studying in the future.

APPENDIX: COMPONENTS OF $T_{\mu\nu}$

The components of $T_{\mu\nu}$ are

$$T^i_{tt}(r,\theta) = Am_0^5 \iiint_{V_i} \frac{\varepsilon^2 e^{-\bar{\beta}\varepsilon}|\cos\theta|}{2\sqrt{\bar{R}}} d\sigma d\varepsilon d\bar{\tau}, \quad \text{(A1)}$$

$$T^i_{tr}(r,\theta) = Am_0^5 \iiint_{V_i} \frac{\varepsilon e^{-\bar{\beta}\varepsilon}|\cos\theta|}{2\Delta} d\sigma d\varepsilon d\bar{\tau}, \quad \text{(A2)}$$

$$T^i_{t\theta}(r,\theta) = Am_0^5 \iiint_{V_i} \frac{\bar{X}\varepsilon e^{-\bar{\beta}\varepsilon}\cos\sigma\cos^2\theta}{2\sqrt{\bar{R}}\sin\theta} d\sigma d\varepsilon d\bar{\tau}, \quad \text{(A3)}$$

$$T^i_{t\varphi}(r,\theta) = -Am_0^5 \iiint_{V_i} \frac{\varepsilon \bar{X} e^{-\bar{\beta}\varepsilon}\sin\sigma|\cos\theta|}{2\sqrt{\bar{R}}} d\sigma d\varepsilon d\bar{\tau}, \quad \text{(A4)}$$

$$T^i_{rr}(r,\theta) = Am_0^5 \iiint_{V_i} \frac{\sqrt{\bar{R}} e^{-\bar{\beta}\varepsilon}|\cos\theta|}{2\Delta^2} d\sigma d\varepsilon d\bar{\tau}, \quad \text{(A5)}$$

$$T^i_{r\theta}(r,\theta) = Am_0^5 \iiint_{V_i} \frac{\bar{X} e^{-\bar{\beta}\varepsilon}\cos\sigma\cos\theta^2}{2\Delta\sin\theta} d\sigma d\varepsilon d\bar{\tau}, \quad \text{(A6)}$$

$$T^i_{r\varphi}(r,\theta) = -Am_0^5 \iiint_{V_i} \frac{\bar{X} e^{-\bar{\beta}\varepsilon}\sin\sigma\cos\theta}{2\Delta} d\sigma d\varepsilon d\bar{\tau}, \quad \text{(A7)}$$

$$T^i_{\theta\theta}(r,\theta) = Am_0^5 \iiint_{V_i} \frac{\bar{X}^2 e^{-\bar{\beta}\varepsilon}\cos^2\sigma|\cos^3\theta|}{2\sqrt{\bar{R}}\sin^2\theta} d\sigma d\varepsilon d\bar{\tau}, \quad \text{(A8)}$$

$$T^i_{\theta\varphi}(r,\theta) = -Am_0^5 \iiint_{V_i} \frac{\bar{X}^2 e^{-\bar{\beta}\varepsilon}\sin\sigma\cos\sigma\cos^2\theta}{2\sqrt{\bar{R}}\sin\theta} d\sigma d\varepsilon d\bar{\tau}, \quad \text{(A9)}$$

$$T^i_{\varphi\varphi}(r,\theta) = Am_0^5 \iiint_{V_i} \frac{\bar{X}^2 e^{-\bar{\beta}\varepsilon}\sin^2\sigma|\cos\theta|}{2\sqrt{\bar{R}}} d\sigma d\varepsilon d\bar{\tau}, \quad \text{(A10)}$$

where i stands for absorption or scattering. The domain V_i of integration is determined by the case of absorption or scattering. For the absorption part, the intervals are $\sigma \in [-\frac{\pi}{2}, \frac{\pi}{2}], \varepsilon \in [1, \infty)$, and $\bar{\tau} \in [0, \bar{\tau}_c]$. For the scattering part, the intervals are $\sigma \in [-\frac{\pi}{2}, \frac{\pi}{2}], \varepsilon \in [\varepsilon_{\min}, \infty)$, and $\bar{\tau} \in [\bar{\tau}_c, \bar{\tau}_{\max}]$.

[1] A. M. Fridman and V. L. Polyachenko, *Physics of Gravitating Systems I: Equilibrium and Stability* (Springer Science & Business Media, Berlin, 2012).

[2] J. Binney and S. Tremaine, *Galactic Dynamics* (Princeton University Press, Princeton, NJ, 2011), Vol. 20.

[3] E. Ames, H. Andréasson, and O. Rinne, On the hoop conjecture and the weak cosmic censorship conjecture for the axisymmetric Einstein-Vlasov system, Phys. Rev. D **108**, 064054 (2023).

[4] S. Günther, J. Körner, T. Lebeda, B. Pötzl, G. Rein, C. Straub, and J. Weber, A numerical stability analysis for the Einstein–Vlasov system, Classical Quantum Gravity **38**, 035003 (2020).

[5] S. Günther, C. Straub, and G. Rein, Collisionless equilibria in general relativity: Stable configurations beyond the first binding energy maximum, Astrophys. J. **918**, 48 (2021).

[6] G. Rein, Stability and instability results for equilibria of a (relativistic) self-gravitating collisionless gas–a review, Classical Quantum Gravity **40**, 193001 (2023).

[7] B. R. Ryan, S. M. Ressler, J. C. Dolence, C. Gammie, and E. Quataert, Two-temperature GRRMHD simulations of M87, Astrophys. J. **864**, 126 (2018).

[8] K. Akiyama, A. Alberdi, W. Alef, K. Asada *et al.*, First M87 event horizon telescope results. I. The shadow of the supermassive black hole, Astrophys. J. **875**, L1 (2019).

[9] K. Akiyama, A. Alberdi, W. Alef, K. Asada, R. Azulay, A. Baczko, D. Ball, M. Baloković, J. Barrett, and D. Bintley, First M87 event horizon telescope results. V. Physical origin of the asymmetric ring, Astrophys. J. **875**, L5 (2019).

[10] K. Akiyama, A. Alberdi, W. Alef, J. C. Algaba, R. Anantua, K. Asada, R. Azulay, U. Bach, A.-K. Baczko, D. Ball *et al.*, First sagittarius a* event horizon telescope results. I. The shadow of the supermassive black hole in the center of the Milky Way, Astrophys. J. Lett. **930**, L12 (2022).

[11] K. Akiyama, A. Alberdi, W. Alef, J. C. Algaba, R. Anantua, K. Asada, R. Azulay, U. Bach, A.-K. Baczko, D. Ball *et al.*, First sagittarius a* event horizon telescope results. V. Testing astrophysical models of the galactic center black hole, Astrophys. J. Lett. **930**, L16 (2022).

[12] P. Rioseco and O. Sarbach, Accretion of a relativistic, collisionless kinetic gas into a Schwarzschild black hole, Classical Quantum Gravity **34**, 095007 (2017).

[13] P. Rioseco and O. Sarbach, Spherical steady-state accretion of a relativistic collisionless gas into a Schwarzschild black hole, J. Phys. Conf. Ser. **831**, 012009 (2017).

[14] F. Hoyle and R. A. Lyttleton, The effect of interstellar matter on climatic variation, Math. Proc. Cambridge Philos. Soc. **35**, 405 (1939).

[15] R. Lyttleton and F. Hoyle, The evolution of the stars, Nature (London) **146**, 97 (1940).

[16] H. Bondi and F. Hoyle, On the mechanism of accretion by stars, Mon. Not. R. Astron. Soc. **104**, 273 (1944).

[17] E. Chaverra and O. Sarbach, Radial accretion flows on static spherically symmetric black holes, Classical Quantum Gravity **32**, 155006 (2015).

[18] A. Cieślik and P. Mach, Accretion of the Vlasov gas on Reissner-Nordström black holes, Phys. Rev. D **102**, 024032 (2020).

[19] P. Mach and A. Odrzywołek, Accretion of dark matter onto a moving Schwarzschild black hole: An exact solution, Phys. Rev. Lett. **126**, 101104 (2021).

[20] P. Mach and A. Odrzywołek, Accretion of the relativistic Vlasov gas onto a moving Schwarzschild black hole: Exact solutions, Phys. Rev. D **103**, 024044 (2021).

[21] P. Mach and A. Odrzywolek, Accretion of the relativistic Vlasov gas onto a moving Schwarzschild black hole: Low-temperature limit and numerical aspects, Acta Phys. Pol. B Proc. Suppl. **15**, 1 (2022).

[22] A. Gamboa, C. Gabarrete, P. Domínguez-Fernández, D. Núñez, and O. Sarbach, Accretion of a Vlasov gas onto a black hole from a sphere of finite radius and the role of angular momentum, Phys. Rev. D **104**, 083001 (2021).

[23] J. Liao and D.-J. Liu, Accretion of the relativistic Vlasov gas onto a bardeen regular black hole, Astrophys. Space Sci. **367**, 109 (2022).

[24] Z. Cai and R.-J. Yang, Accretion of the Vlasov gas onto a Schwarzschild-like black hole, Phys. Dark Universe **42**, 101292 (2023).

[25] P. Rioseco and O. Sarbach, Phase space mixing in the equatorial plane of a Kerr black hole, Phys. Rev. D **98**, 124024 (2018).

[26] L. Andersson, P. Blue, and J. Joudioux, Hidden symmetries and decay for the Vlasov equation on the Kerr spacetime, Commun. Partial Differ. Equations **43**, 47 (2018).

[27] A. Cieślik, P. Mach, and A. Odrzywołek, Accretion of the relativistic Vlasov gas in the equatorial plane of the Kerr black hole, Phys. Rev. D **106**, 104056 (2022).

[28] P. Mach and A. Odrzywołek, Equatorial accretion on the Kerr black hole, Acta Phys. Pol. B Proc. Suppl. **16**, 13 (2023).

[29] B. Carter, Republication of: Black hole equilibrium states: Part I analytic and geometric properties of the Kerr solutions, Gen. Relativ. Gravit. **41**, 2873 (2009).

[30] S. Chandrasekhar, *The Mathematical Theory of Black Holes* (Oxford University Press, New York, 1998), Vol. 69.